Effect of A-Zeolite on the Crystallization Behavior of *In-situ* Polymerized Poly(ethylene terephthalate) (PET) Nanocomposites

Young Hak Shin, Wan Duk Lee, and Seung Soon Im*

Department of Fiber & Polymer Engineering, College of Engineering, Hanyang University, Seoul 133-791, Korea

Abstract: The crystallization behavior and fine structure of poly(ethylene terephthalate) (PET)/A-zeolite nanocomposites were assessed via differential scanning calorimetry (DSC) and time-resolved small-angle X-ray scattering (TR-SAXS). The Avrami exponent increased from 3.5 to approximately 4.5 with increasing A-zeolite contents, thereby indicating a change in crystal growth formation. The rate constant, k, evidenced an increasing trend with increases in A-zeolite contents. The SAXS data revealed morphological changes occurring during isothermal crystallization. As the zeolite content increased, the long period and amorphous region size also increased. It has been suggested that, since PET molecules passed through the zeolite pores, some of them are rejected into the amorphous region, thereby resulting in increased amorphous region size and increased long period, respectively. In addition, as PET chains piercing into A-zeolite pores cannot precipitate perfect crystal folding, imperfect crystals begin to melt at an earlier temperature, as was revealed by the SAXS profiles obtained during heating. However, the spherulite size was reduced with increasing nanofiller content, because impingement between adjacent spherulites in the nanocomposite occurs earlier than that of homo PET, due to the increase in nucleating sites.

Keywords: PET, A-zeolite, nanocomposite, crystallization behavior, fine structure.

Introduction

Poly(ethylene terephthalate) (PET) is a thermoplastic polyester widely used in the manufacture of high-strength fibers, photographic films, and soft-drink bottles owing to its good mechanical properties with low cost.[1] However, PET has some drawbacks on the processability due to the relatively slow crystallization rate. Accordingly, studies on the PET nanocomposites filled with inorganic materials have been investigated for the enhancement of their processability and properties.[2-6]

Zeolites are microporous crystalline aluminosilicates and composed TO_4 tetrahedra (T = Si, Al) with oxygen atoms connecting neighboring tetrahedra.[7] Zeolites have potential applications such as catalysts, adsorption agents, and ion-exchange resins on account of their regular pore structures and high thermal stability. They were also employed as an additive to impart antibacterial and flame retardant properties to polymers. LTA type A-zeolite having Si/Al ratio of 1, sodium ions as a counter ion, a pore size larger than 4 Å, and primary particle size of 10-30 nm were used as nanocomposite fillers in this study. Their general chemical formula is $Na_{96}(Si_{96}Al_{96}O_{384})$ possessing SiO_4^-, AlO_4^- as basic

units. Recently, these zeolites were used to polymer composite system as fillers, which play a role of reinforcement filler and nucleating agent.[8]

In the polymer/zeolite nanocomposites, there are two controversial reports about effects of zeolite on the composite properties. One report[9] is that the incorporated zeolites decrease the mechanical properties of polymer due to poor interfacial interactions between polymer and zeolite. The other report is that zeolite bring on reinforcing effects on the polymer, such as mechanical properties and crystallization behavior, because polymer chains could pass through zeolite pores in the nanocomposites. In particular, Frisch et al.[10-12] prepared interpenetrating polymer network (IPN) of zeolite 13X and polystyrene or polyethylacrylate, which prepared by using *in-situ* radical polymerization. In addition, Bein and Wu reported about preparation of molecular wires and conducting polyaniline filaments from polymer chains constrained into zeolite pores.[13,14]

In this paper, PET/A-zeolite nanocomposites were prepared by using *in-situ* polymerization, which could be applied as an effective method for improvement of zeolite filler dispersion. And then the effects of A-zeolite loading on isothermal crystallization kinetics, melting behavior, and crystalline structure were investigated and discussed briefly.

*Corresponding Author. E-mail: imss007@hanyang.ac.kr

Experimental

Materials and Preparation of Nanocomposites. PET nanocomposites containing A-zeolites (0-2.0 wt%) used in this study were prepared by using *in-situ* polymerization. *In-situ* polymerization method is advantageous because it produces a homogeneous dispersion of A-zeolite particles in the polymer matrix.[15] Dimethyl terephthalate (DMT) and Ethylene glycol (EG) (+ 99%) purchased from Sigma-Aldrich were used without further purification. A-zeolites were kindly supplied from Korea Institute of Ceramic Eng. & Tech. (KICET). PET/A-zeolite nanocomposites were prepared by conventional two-step polycondensation. A-zeolites and zinc-acetate catalyst were firstly dispersed in EG solution by Ultra sonic vibration for 10 min before ester interchange reaction. During this process, the EG monomer and catalyst can effectively incorporate into A-zeolite pores. EG slurry was then mixed with DMT, and temperature was slowly increased to 210 °C with stirring. Finally, Ester interchange reaction was carried out for 3 h with continuously removing byproduct (methanol). Second polycondensation reaction was carried out at temperatures ranging from 180 to 285 °C with typical antimony oxide catalyst under vacuum below 0.1 torr for 2 h. The synthesized all of the nanocomposite samples were dried *in vacuum* for 24 h at 70 °C.

Characterizations of Nanocomposites.

Isothermal Crystallization: The isothermal crystallizations and melting behaviors of the PET/A-zeolite nanocomposites were measured using a Perkin-Elmer DSC 7 instrument in a nitrogen atmosphere. The nanocomposite samples were heated to 300 °C, kept for 5 min to eliminate thermal history, and then cooled rapidly (200 °C/min) to the crystallization temperature within the range of 190-220 °C and maintained for 30 min. During isothermal crystallization, exothermic heat flow was recorded as a function of time at a different crystallization temperature. After crystallization, the fully crystallized samples were cooled down to 40 °C at a rate of 200 °C/min, and then second heating run was carried out at a rate of 10 °C/min.

Synchrotron X-Ray Scattering Measurements: Synchrotron X-ray scattering experiments were carried out at the 4C2 SAXS beam line of the Pohang Accelerater Laboratory (Pohang, Korea). The X-ray wavelength (λ) used was 0.154 nm and the beam size at the focal point was less than 1 mm², focused by platinum coated silicon premirror through a double crystal monochromator. The scattering intensity was detected with a two-dimensional CCD camera. The scattering angle was calculated with a Bragg spacing of 32.5 nm for a SEBS crystal at $q = 0.1933$ nm⁻¹ as a reference peak for SAXS. The samples were completely melted at 300 °C to remove their any thermal history in the melting chamber, and then they were quickly moved into the crystallization chamber set to same isothermal crystalli-

zation temperatures mentioned above.

SAXS Data Analysis: All SAXS data were corrected for the background, including a dark current and air scattering, and were plotted as a Lorentz-corrected form, Iq^2 against q, where q is the scattering vector given by the following form:

$$q = \frac{4\pi}{\lambda}\sin\theta \qquad (1)$$

where λ is the wavelength and θ is the scattering angle. The morphological parameters, such as the long period, average lamellar thickness, and amorphous region size, were calculated from the one-dimensional correlation function $G(r)$ by assuming ideal two-phase model.

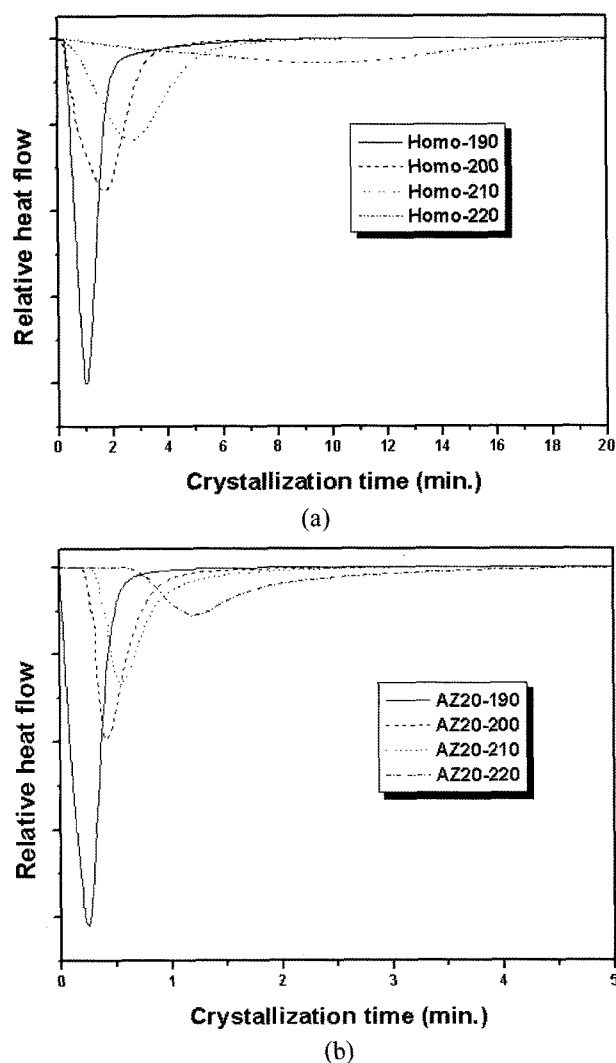$$G(r) = \left(\frac{1}{2\pi}\right)^2 \int q^2 I(q)\cos(qr)dq \qquad (2)$$

Figure 1. DSC isothermograms of (a) homo PET and (b) nanocomposite filled with 2.0 wt% A-zeolite (AZ20).

where r is the correlation distance. The long period (L) was determined from the first maximum of the correlation curve. The average lamellar thickness (l_c) was determined from the x-axis values of an intersection point between the tangent-line at $G(r) = 0$ and the tangent-line at the first minimum in the correlation curve. The size of amorphous region (l_a) was obtained by L and l_c ($l_a = L - l_c$).

Results and Discussion

Avrami Theory Analysis. The isothermal crystallization exotherms of the nanocomposite samples are shown in Figure 1. The relative crystallinity, X_t, was obtained from the ratio of the area of the exotherm up to time t divided by the total exotherm. The development of the relative crystallinity with time of the nanocomposite samples is shown in Figure 2. All isotherms exhibited a sigmoidal dependence on time. The crystallization rate of the nanocomposite samples increased with increasing A-zeolite contents. It is indicated

that A-zeolite can be acted as a heterogeneous nucleation agent in the PET matrix. In addition, the crystallization rate of every sample showed a decreasing trend with increasing the crystallization temperature.

The crystallization kinetics of the nanocomposite samples were analyzed by using typical Avrami equation,[16,17] which can be expressed as the following form:

$$1 - X_t = \exp(-kt^n) \tag{3}$$

where k is the temperature-dependent rate constant, t is the crystallization time, and n is the Avrami exponent, indicating the type of nucleation and dimension of crystal growth.

Taking logarithms, eq. (3) can be expressed as the following form:

$$\log[-\ln(1 - X_t)] = n\log t + \log k \tag{4}$$

Here, n and k are obtained from the slope and intercept of the linear plot of $\log(-\ln(1 - X_t))$ against $\log(t)$ in the primary crystallization portion, respectively. The plots of log
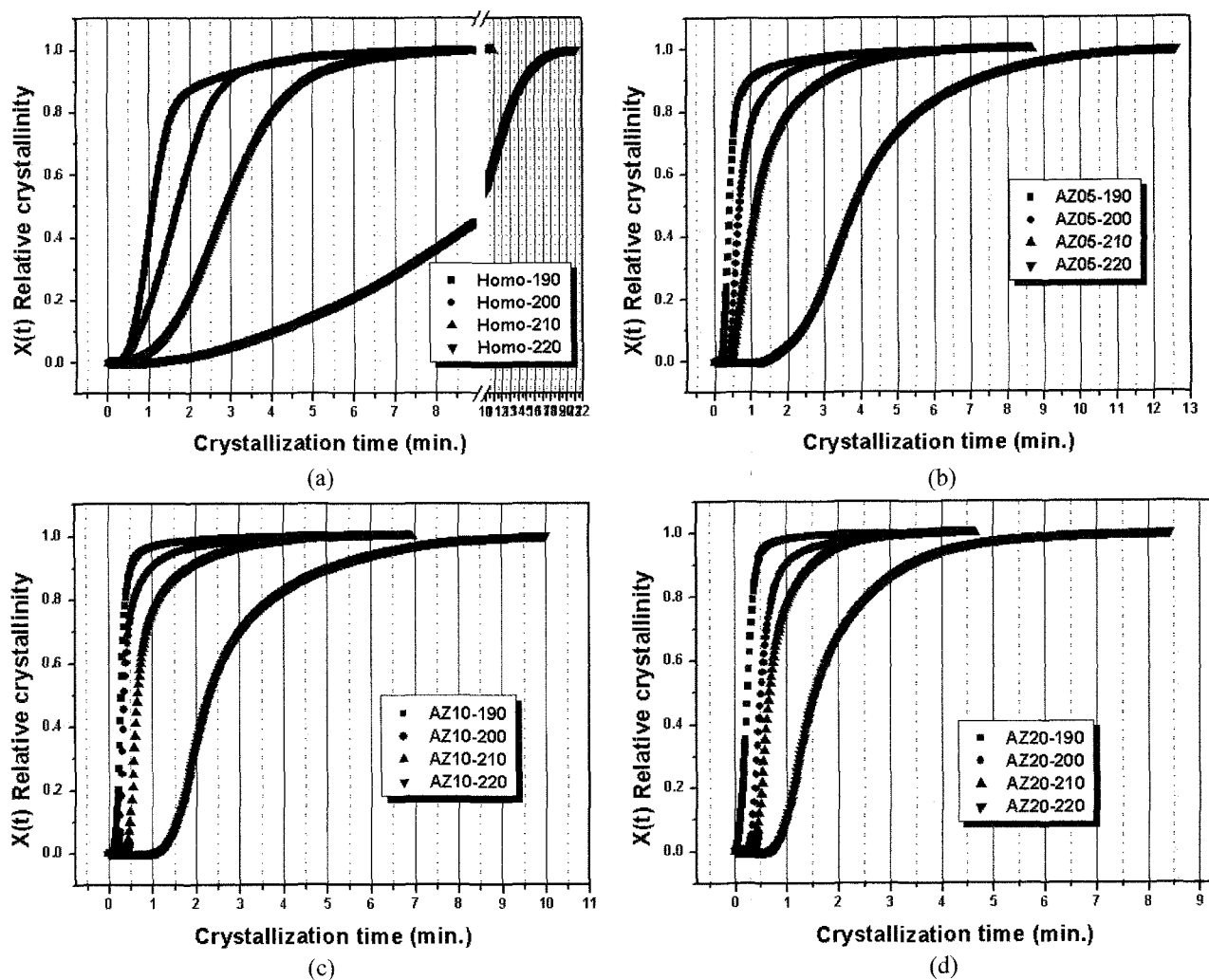

Figure 2. Relative crystallinity versus time of the nanocomposites; (a) homo PET, (b) AZ05, (c) AZ10, and (d) AZ20.
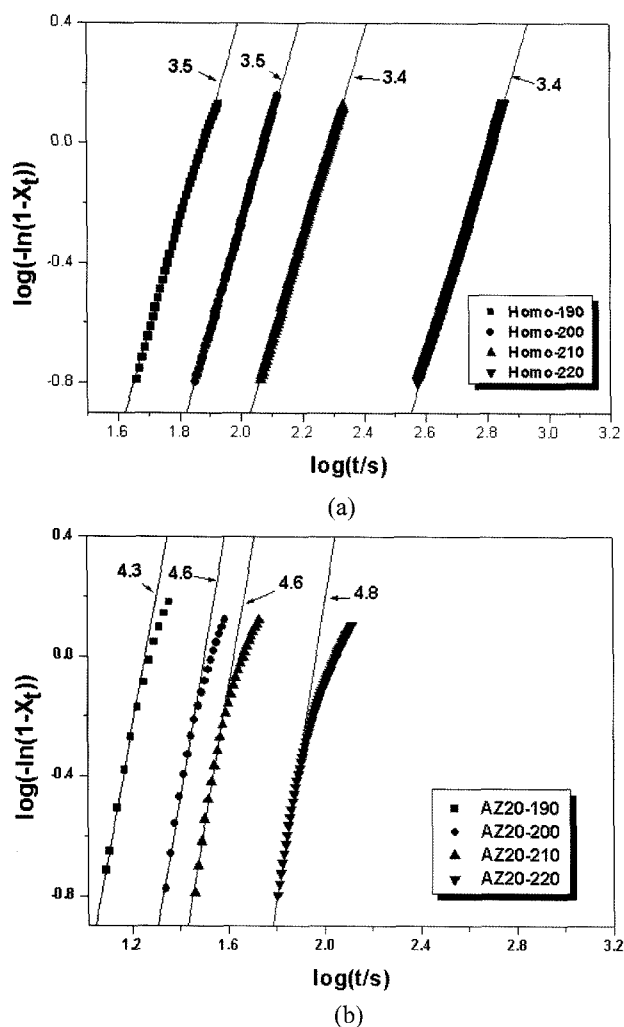
Figure 3. Avrami plots for (a) homo PET and (b) AZ20 nanocomposite crystallized at various temperatures.

Table I. The Avrami Parameters for the Various Crystallization Temperatures

Sample	n	K (s^{-n})	$t_{1/2}$ (sec)
Homo-190	3.5	1.013×10^{-6}	66.6
200	3.5	1.594×10^{-6}	103.2
210	3.4	1.357×10^{-7}	172.2
220	3.4	1.327×10^{-8}	570.6
AZ05-190	3.9	2.373×10^{-6}	25.2
200	4	2.359×10^{-7}	41.4
210	4.2	1.400×10^{-8}	67.8
220	4.3	4.756×10^{-11}	231
AZ10-190	4	7.561×10^{-6}	17.4
200	4.6	5.039×10^{-7}	21.6
210	4.8	1.382×10^{-8}	40.2
220	4.7	5.831×10^{-11}	139.2
AZ20-190	4.3	7.242×10^{-6}	14.4
200	4.6	1.112×10^{-7}	30
210	4.6	2.893×10^{-8}	40.2
220	4.8	2.319×10^{-10}	94.2
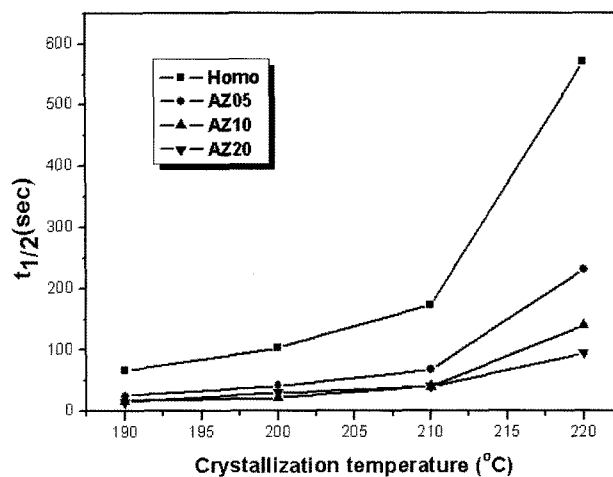
Figure 4. Half-time of crystallization versus crystallization temperature.

$(-\ln(1 - X_t))$ against $\log(t)$ for the nanocomposite samples are shown in Figure 3. The plots of all samples shifted toward longer times with increasing the crystallization temperature. It is indicated that the time to reach the maximum crystallinity increased as the crystallization temperature increases. The Avrami kinetic parameters are listed in Table I. The n values for homo PET lies in the nearly 3.5. On the other hand, the n values for the nanocomposite samples have higher value than that of homo PET. In addition, when the n values between nanocomposite samples were compared with each other, the n value increased slightly with increasing A-zeolite contents at the range of 4-5. It indicates that crystal growth dimension of nanocomposites is more complicate than that of homo PET. The rate constant, k, shows a very temperature-sensitive decrease in all samples, and k values increase with increasing A-zeolite contents.

The half-time of crystallization, $t_{1/2}$, can be useful indicator of the crystallization rate. Usually, the reciprocal of $t_{1/2}$ is

used to describe the crystallization rate, $G = (t_{1/2})^{-1}$. The greater value of $t_{1/2}$ means the slower crystallization rate. The $t_{1/2}$ for all samples is shown in Figure 4. The incorporation of A-zeolites decreased the $t_{1/2}$ of the PET matrix, indicating the nucleating effect of A-zeolites for PET. Furthermore, the value of $t_{1/2}$ is less dependent on temperature with increasing A-zeolite contents. Thus, A-zeolite acts as heterogeneous nucleating agent. The half time of crystallization is listed in Table I.

Crystallization Activation Energy. The crystallization rate constant of Avrami kinetic parameter, k is assumed to be thermally activated and can be used to determine crystallization activation energy (ΔE). The k can be approximately
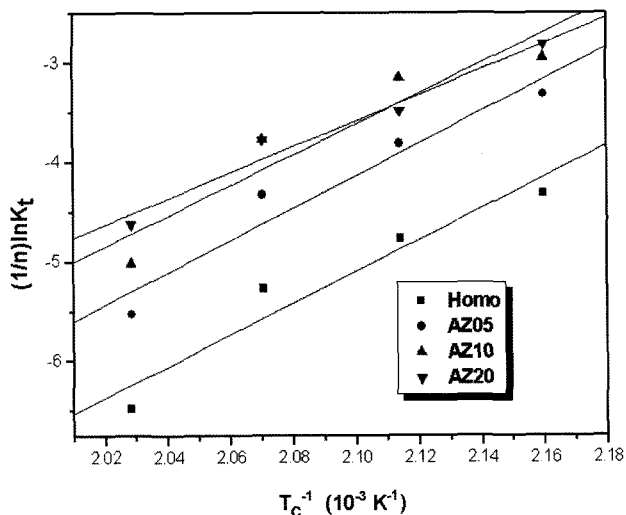
Figure 5. Plots of $(1/n)\ln K_t$ versus $1/T_c$ for Avrami parameter K_t deduced from isothermal crystallization.

Table II. Crystallization Activation Energy of the Nano-composites

Sample	Activation Energy (J/mol)
Homo	-173
AZ05	-158
AZ10	-126
AZ20	-111

described by the Arrhenius equation:[18-20]

$$k_t^{1/n} = k_0 \exp\left(\frac{-\Delta E}{RT_c}\right) \tag{5}$$

Taking logarithms, eq. (5) can be expressed as the following form:

$$\left(\frac{1}{n}\right)\ln k_t = \ln k_0 - \frac{\Delta E}{RT_c} \tag{6}$$

where k_0 is a pre-exponential constant, R is the gas constant, ΔE is the crystallization activation energy, and T_c is the crystallization temperature. Arrhenius plots of $1/n(\ln k)$ against $1/T_c$ for all samples are shown in Figure 5 and are linearly fitted. Here, ΔE can be obtained from the slope of the plots (Table II). ΔE is strongly dependent on A-zeolite contents. ΔE decreased with increasing A-zeolite contents, and drastically decreased over the 2 wt% of A-zeolite. It is indicated that the incorporation of A-zeolite causes a heterogeneous nucleation, which results in a lower ΔE.[18-20] In other words, the crystallization rate can be accelerated during the isothermal crystallization process owing to A-zeolite.

Melting and Equilibrium Melting Temperatures. Figure 6 represents the second heating run thermograms for the completely crystallized samples. In the thermograms of all
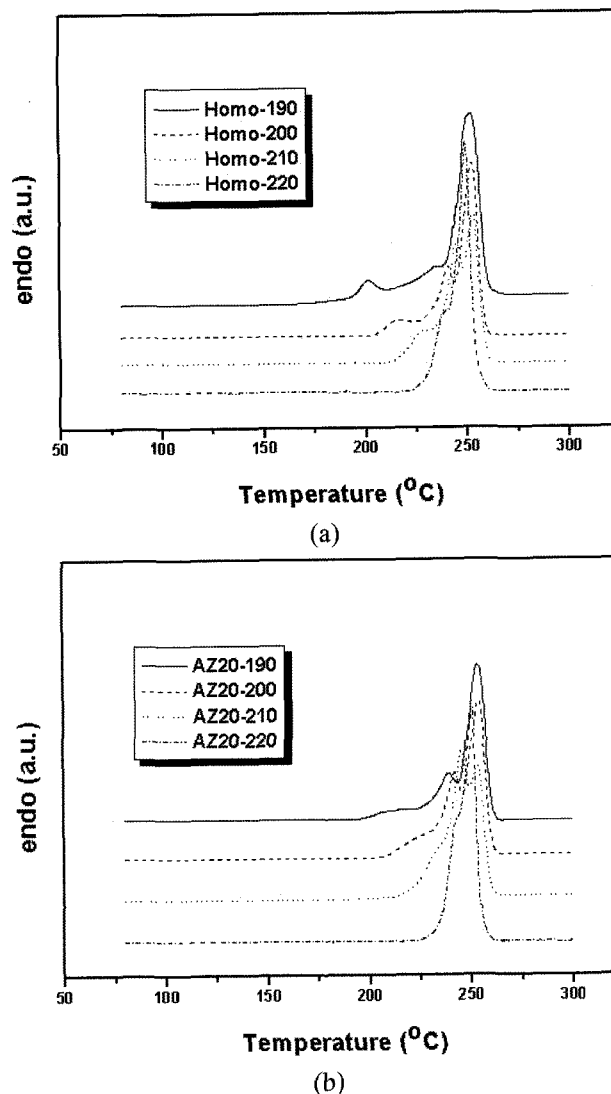

(a)

(b)

Figure 6. DSC second heating runs for the fully crystallized (a) homo PET and (b) AZ20 nanocomposite at various crystallization temperatures.

nanocomposite samples, three melting peaks can be observed. The lowest small melting peak appears at about 10-15 °C above the crystallization temperature,[21,22] which is called annealing peak. The middle melting peak is corresponded to the melting of original crystal lamellae grown during isothermal crystallization, and the highest melting peak is corresponded to the melting of crystallites produced by melt-recrystallization. Accordingly, in this work, the equilibrium melting temperature was obtained by using the middle melting temperature (T_m).

The equilibrium melting temperature, T_m^o is the melting temperature of infinitely stack crystals. It can be obtained as a theory derived by Hoffman-Weeks.[23]

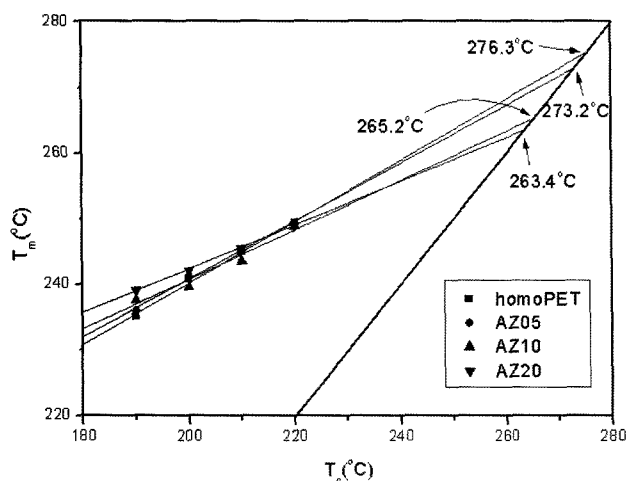$$T_m = \frac{T_c}{\gamma} + \left(1 - \frac{1}{\gamma}\right)T_m^o \tag{7}$$
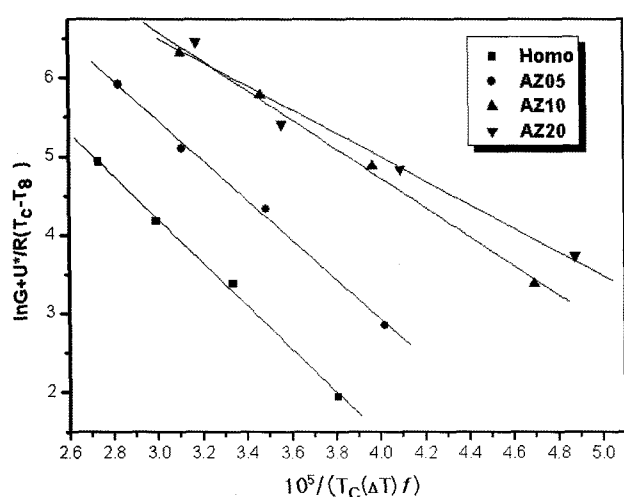
Figure 7. Hoffman-Weeks plots of the nanocomposites.

Figure 8. Lauritzen-Hoffman plots of the nanocomposites.

Table III. The Kinetic Data for Crystallized Nanocomposites

Sample	K_g (K^2)	σ_e (J m^{-2})
Homo	2.75×10^5	10.12×10^{-2}
AZ05	2.53×10^5	9.36×10^{-2}
AZ10	1.86×10^5	6.99×10^{-2}
AZ20	1.51×10^5	5.69×10^{-2}

(a)

(b)
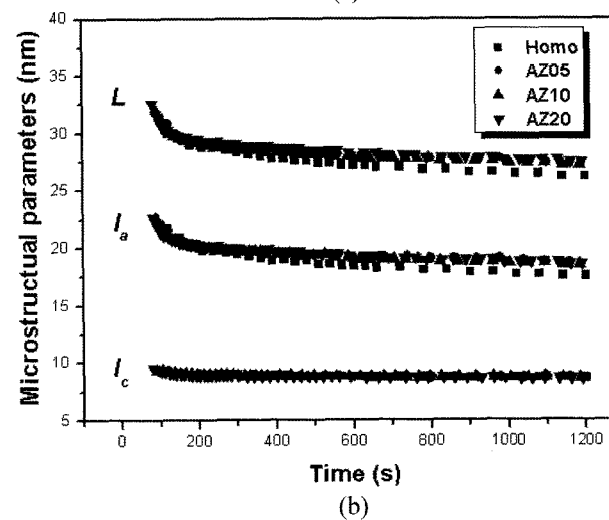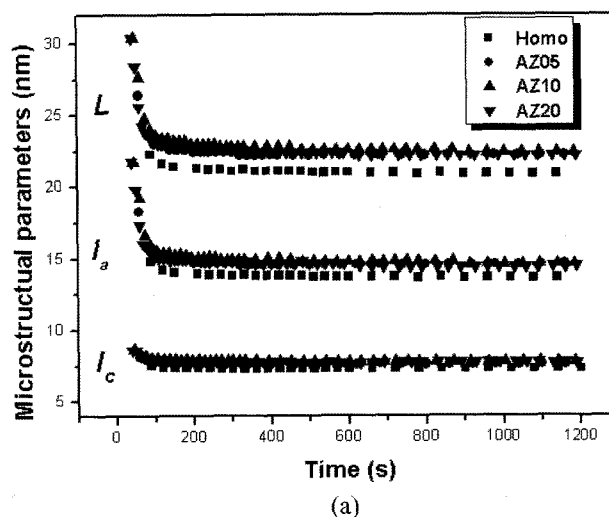
Figure 9. Change of morphological parameters during isothermal crystallization at (a) 190 °C and (b) 220 °C.

where T_m and T_m^o are the experimental melting temperature and equilibrium melting temperature, respectively. T_c is the crystallization temperature and γ is the lamellar thickening ratio, which is supposed to always be greater than or equal to 1.[24,25]

The fitting of T_m against T_c is approximately linear, which is shown in Figure 7. The T_m^o is evaluated by the x-axis value of an intersection of linear line obtained from experimental data and $T_m = T_c$ linear line. The T_m^o decreased with increasing A-zeolite contents. It is suggested that the crystal perfection of the nanocomposite fall off with increasing A-zeolite contents.[26] This result will be also confirmed from SAXS results and will be discussed in detail at following SAXS sections.

Secondary Nucleation Theory Analysis. The crystal growth rates of the spherulite may be derived from the Lauritzen-Hoffman secondary nucleation theory.[24,27] In this

study, the reciprocal of half-crystallization time of isothermal crystallization in DSC measurement was used as the crystal growth rate (G). The temperature dependence of G is given as follows:

$$G = G_0 \exp\left(- \frac{U^*}{R(T_c - T_\infty)}\right) \exp\left(- \frac{K_g}{T_c(\Delta T)f}\right) \tag{8}$$

where G_0 is the front factor, U^* is the activation energy for the segment diffusion to the site of crystallization, R is the

gas constant, T_∞ is the hypothetical temperature below which all viscous flow ceases, K_g is the nucleation parameter, ΔT is the degree of supercooling defined as $T_m^o - T_c$ and f is a correction factor given as $2T_c/(T_m^o + T_c)$. Generally, taking logarithms, eq. (9) can be expressed as the following form:

$$\ln G + \left(\frac{U^*}{R(T_c - T_\infty)}\right) = \ln G_0 - \frac{K_g}{T_c(\Delta T)f} \tag{9}$$

In this study, we used the universal values of $U^* = 6300$ Jmol^{-1} and $T_\infty = T_g - 30$ K in all calculations.[27] With this assumption, K_g value is obtained from the slope of Plots of $\ln G + U^*/R(T_c - T_\infty)$ against $1/T_c(\Delta T)f$ as shown in Figure 8, and can be expressed as the following form:[24,28]

$$K_g = \frac{nb_o\sigma\sigma_e T_m^o}{\Delta h_f \kappa_B} \tag{10}$$

where n is a constant equals to 2 for regime II, b_0 is the monomolecular layer thickness, taken as the unit cell dimension of b, σ is the lateral surface energy, σ_e is the fold surface free

energy, Δh_f is the heat of fusion per unit volume (182.6 Jcm^{-3} = heat of fusion per unit mass (125.5 J/g^{15}) * crystal density (1.455 gcm^{-3}))[39] and κ_B is the Boltzmann constant.

On the other hand, the lateral surface energy, σ was often estimated as:[28]

$$\sigma = \alpha(\Delta h_f)(a_0 b_0)^{1/2} \tag{11}$$

where α was derived empirically to be 0.11 by analogy with the well-known behavior of hydrocarbons. The unit cell dimensions a_0 and b_0 for PET used in this analysis are 4.57 and 5.95 Å, respectively.[29] From eqs. (10) and (11), the fold surface free energy, σ_e can be calculated and was shown in Table III. The σ_e decreases with increasing A-zeolite contents. It is indicated that the work required in folding the molecules decreases with increasing A-zeolite contents.[30] Consequently, it is concluded that the overall crystallization rate was increased by the incorporation of A-zeolite in the PET matrix.[30]

SAXS Studies During Isothermal Crystallization and Melting Process. The changes of morphological parame-
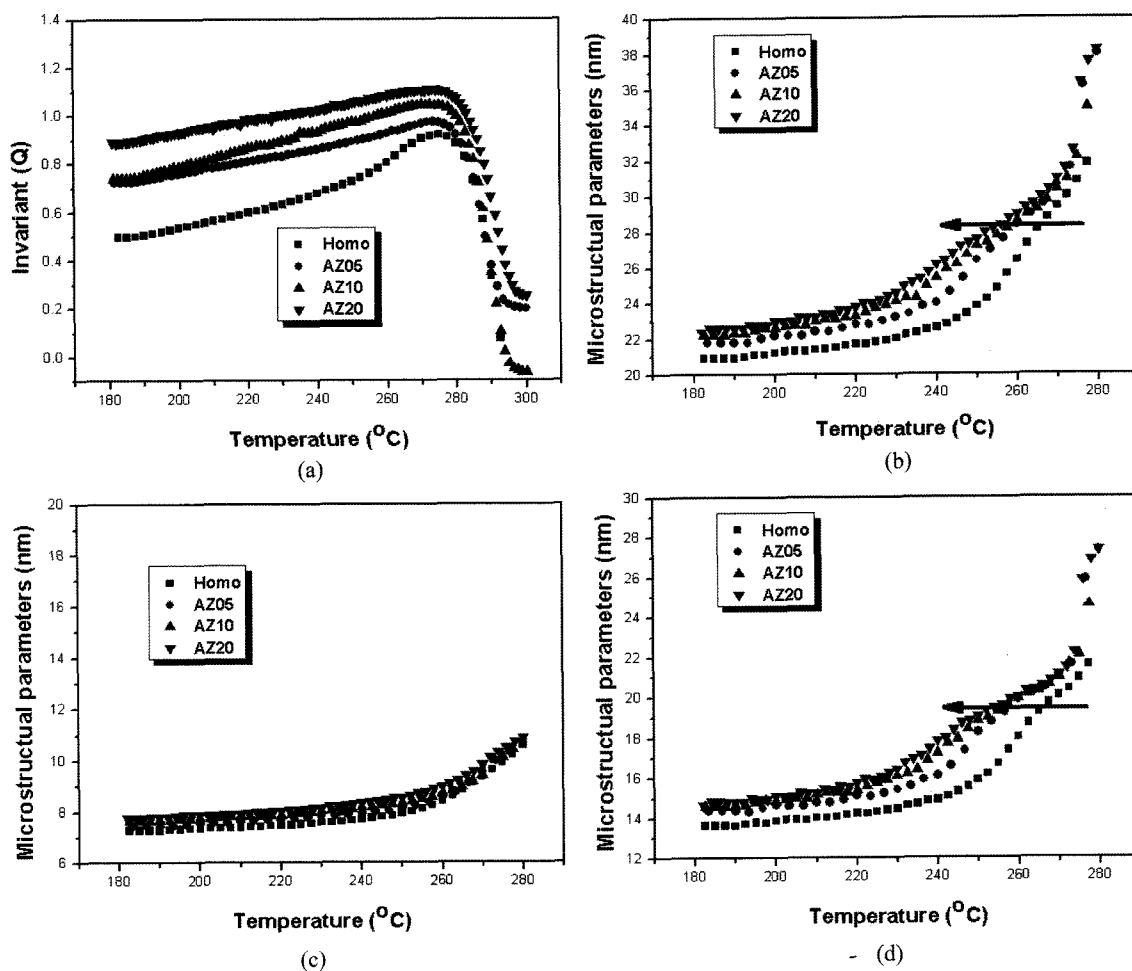

Figure 10. Microstructural parameters during heating after isothermal recrystallization at 190 °C; (a) invariants, (b) long period, (c) average lamellar thickness, and (d) average amorphous size.

ters obtained from linear correlation function curve for nanocomposite samples crystallized at 190 and 220 °C are shown in Figure 9. As crystallization proceeded, L and l_a drastically decreased, especially in the initial crystallization period, at the each crystallization temperature. This could be caused by the insertion of subsidiary lamellae between two existing dominant lamellae.[31-34] As the zeolite filler content increased, l_c for all nanocomposites are almost same, because the lamellar thickness depends not on the nucleation but on the molecular diffusion at a controlled temperature. However, L and l_a increased slightly as the zeolite content increased during isothermal crystallization. This result is opposite to that of PET nanocomposites filled with nano-sized layered materials.[38,39] In the case of nanocomposites filled with layered materials, nanocomposites could be crystallized more easily owing to the increase of nanolayers acted as nucleation site, leading to the decrease of the average amorphous region size. In the case of PET/ zeolite nanocomposite, however, it is believed that PET molecules passed through zeolite pores. Therefore, PET chains piercing zeolite couldn't make appropriate folding and some of them are rejected into amorphous region, leading to the increase of l_a and L, respectively.[35]

Figure 10 shows the change of morphological parameters during heating after the isothermal crystallization at 190 °C for 20 min. As shown in Figure 10(a) and 10(c), invariants (overall scattering power) and l_c for all nanocomposites increased with increasing temperature owing to the crystal thickening. And, invariants decreased abruptly after melting over 275 °C. L and l_a also increased with temperature, indicating the thermal expansion resulting from the increased molecular mobility during heating, as shown in Figure 10(b) and 10(d), respectively. In these figures, interestingly, the temperature of the rapid increase in L and l_a, which resulted from the onset of the crystal melting, was shifted to lower temperature with increasing zeolite content. This result is also opposite to that of nanocomposites filled with layered materials.[38] Based on the decrease of equilibrium melting temperature with zeolite content as shown in Figure 7, it is thought that PET molecules threading into zeolite pores couldn't make perfect crystal[36,37] during isothermal crystallization, leading to the decrease of those onset temperature of crystal melting. Schematic diagram of lamellar structures and spherulite for the isothermally crystallized PET and PET/A-zeolite nanocomposites are presented in Figure 11. It is believed that since PET molecules threading into A-zeolite pores cannot make perfect crystal folding, imperfect crystal start to melt at earlier temperature. In addition, L and l_a increased with increasing zeolite content because some of them are rejected into amorphous region during crystallization, while l_c was almost same. Accordingly, based on the above results, the changes of morphological parameters for nanocomposite samples were resulted from the molecular threading. However, spherulite size decreased with increas-
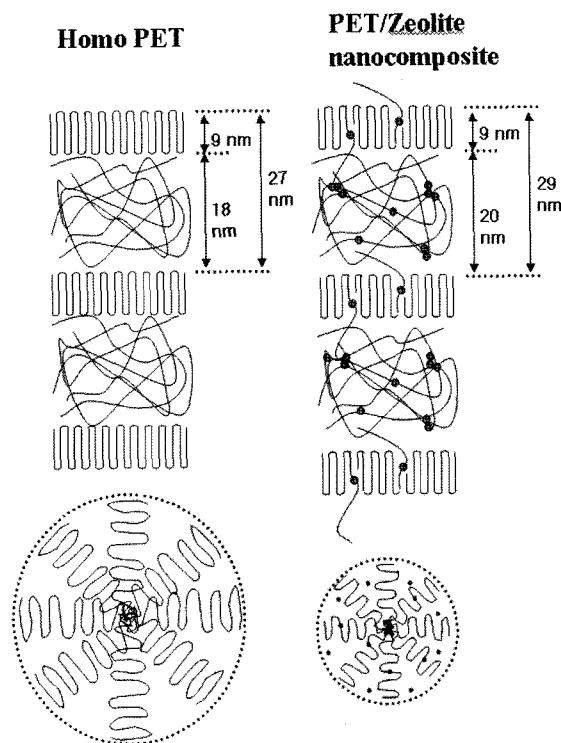

Figure 11. Schematic diagrams of the nanocomposite crystal.

ing nanofiller content, because impingement between adjacent spherulites in the nanocomposite occurs earlier than that of homo PET owing to the increased nucleating site.

Conclusions

The PET/A-zeolite nanocomposites were prepared successfully by *in-situ* polymerization. DSC analysis suggested that crystallization rates of the nanocomposite samples were increased because A-zeolites acted as nucleating agents. The evolution of crystallization kinetics during isothermal crystallization and subsequent melting was followed by time-resolved SAXS and DSC measurements. It indicated that the crystallization growth rates of the nanocomposite samples increased with increasing A-zeolite contents. However, the crystals of nanocomposite formed less perfect crystals owing to molecular threading of PET chains into A-zeolite pores. It is confirmed from decreased equilibrium melting temperatures and SAXS analysis. Since PET molecules threading into A-zeolite pores couldn't make perfect crystal folding, and some of them were rejected into amorphous region, amorphous region size and long period were increased.

References

(1) R. Sareen and S. K. Gupta, *J. Appl. Polym. Sci.*, **58**, 2357 (1994).

(2) G. Zhang, T. Shichi, and K. Takagi, *Mater. Lett.*, **57**, 1858 (2003).

(3) Y. Wang, C. Shen, H. Li, Q. Li, and J. Chen, *J. Appl. Polym. Sci.*, **91**, 308 (2004).

(4) W. Liu, X. Tian, P. Cui, Y. Li, K. Zheng, and Y. Yang, *J. Appl. Polym. Sci.*, **91**, 1229 (2004).

(5) Y. C. Ke, Z. B. Yang, and C. F. Zhu, *J. Appl. Polym. Sci.*, **85**, 2677 (2002).

(6) J. H. Chang, S. J. Kim, Y. L. Joo, and S. S. Im, *Polymer*, **24**, 919 (2004).

(7) S. M. Auerbach, K. A. Carrado, and P. K. Dutta, *Handbook of Zeolite Science and Technology*, Marcel Dekker, New York, 2003, p 85.

(8) H. Pehlivan, D. Balkose, S. Ulku, and F. Tihminlioglu, *Compos. Sci. Technol.*, **65**, 2049 (2005)

(9) F. Özmihçl, D. Balköse, and S. Ülkü, *J. Appl. Polym. Sci.*, **82**, 2913 (2001).

(10) H. L. Frisch, S. Maaref, Y. Xue, G. Beaucage, Z. Pu, and J. E. Mark, *J. Polym. Sci.*, **34**, 673 (1996).

(11) H. L. Frisch, Y. Xue, and S. Maaref, *Macromol. Symp.*, **106**, 147 (1996).

(12) H. L. Frisch and J. E. Mark, *Chem. Mater.*, **8**, 1735 (1996).

(13) C. G. Wu and T. Bein, *Science*, **264**, 1757 (1994).

(14) C. G. Wu and T. Bein, *Science*, **266**, 1013 (1994).

(15) W. G. Hahm, H. S. Myung, and S. S. Im, *Macromol. Res.*, **12**, 85 (2004).

(16) M. J. Avrami, *Chem. Phys.*, **7**, 1103 (1939).

(17) M. J. Avrami, *Chem. Phys.*, **8**, 212 (1940).

(18) M. Run, S. Wu, D. Zhang, and G. Wu, *Polymer*, **46**, 5308 (2005).

(19) T. M. Wu and C. Y. Liu, *Polymer*, **46**, 5621 (2005).

(20) W. Weng, G. Chen, and D. Wu, *Polymer*, **44**, 8119 (2003).

(21) S. Z. D. Cheng and B. Wunderlich, *Macromolecules*, **21**, 789 (1988).

(22) I. Y. Phang, K. Pramoda, T. Liu, and C. He, *Polym. Int.*, **53**, 1282 (2004).

(23) J. D. Hoffman and J. J. Weeks, *J. Res. Nat. Bur. Stand*, **66A**, 13 (1962).

(24) J. D. Hoffman and R. L. Miller, *Polymer*, **38**, 3151 (1997).

(25) H. Marand, J. Xu, and S. Srinivas, *Macromolecules*, **31**, 8219 (1998).

(26) F. Avalos, M. A. Lopez-Manchado, and M. Arroyo, *Polymer*, **39**, 6173 (1998).

(27) J. D. Hoffman, G. T. Davis, and J. I. Lauritzen, in *Treatise on Solid State Chemistry*, N. B. Hannay, Ed., Plenum Press, New York, Chapter 7, 1976.

(28) W. D. Lee, E. S. Yoo, and S. S. Im, *Polymer*, **44**, 6617 (2003).

(29) X. F. Lu and J. N. Hay, *Polymer*, **42**, 9423 (2001).

(30) J. Ma, S. Zhang, Z. Qi, G. Li, and Y. Hu, *J. Appl. Polym. Sci.*, **83**, 1978 (2002).

(31) R. Verma, H. Marand, and B. S. Hsiao, *Macromolecules*, **29**, 7767 (1996).

(32) K. N. Krüger and H. G. Zachmann, *Macromolecules*, **26**, 5202 (1993).

(33) B. S. Hsiao, K. H. Gardner, D. Q. Wu, and B. Chu, *Polymer*, **34**, 3986 (1993).

(34) B. S. Hsiao, K. H. Gardner, D. Q. Wu, and B. Chu, *Polymer*, **34**, 3996 (1993).

(35) W. D. Lee and S. S. Im, *J. Polym. Sci.; Part B: Polym. Phys.*, **43**, 805 (2005).

(36) C. Fougnies, P. Damman, M. Dosiere, and M. H. J. Koch, *Macromolecules*, **30**, 1392 (1997).

(37) R. Verma, V. Velikov, R. G. Kander, H. Marand, B. Chu, and B. S. Hsiao, *Polymer*, **37**, 5357 (1996).

(38) W. D. Lee and S. S. Im, *J. Polym. Sci.; Part B: Polym. Phys.*, **45**, 28 (2007).

(39) R. de Daubeny, C. W. Bunn, and C. J. Brown, *Proc. Roy. Soc. (London)*, **A226**, 531 (1954).